

Article

Creation of Optimal Frequency for Electrostatic Force Microscopy Using Direct Digital Synthesizer

Seunghyun Moon ^{1,2}, Mingyu Kang ², Jung-Hwan Kim ³, Kyeo-Reh Park ⁴ and ChaeHo Shin ^{1,*}

¹ Division of Industrial Metrology, Korea Research Institute of Standards and Science, Daejeon 34113, Korea; irus7711@snu.ac.kr

² Department of Nano Science and Technology, Graduate School of Convergence Science and Technology, Seoul National University, Seoul 08826, Korea; whitymk@snu.ac.kr

³ Mass Spectrometry & Advanced Instrumentation Group, Korea Basic Science Institute, Cheongju 28119, Korea; jhkim1002@kbsi.re.kr

⁴ Nuclear Fusion & Plasma Laboratory, Korea Advanced Institute of Science and Technology, Daejeon 34141, Korea; parkyere@kaist.ac.kr

* Correspondence: chaeho.shin@kriss.re.kr; Tel.: +82-42-868-5835

Academic Editor: Giorgio Biasiol

Received: 19 May 2017; Accepted: 5 July 2017; Published: 8 July 2017

Abstract: Electrostatic force microscopy (EFM) is a useful technique when measuring the surface electric potential of a substrate regardless of its topography. Here, we have developed a frequency detection method for alternating current (AC) bias in EFM. Instead of an internal lock-in amplifier (LIA) for EFM that only detects ω_e and $2\omega_e$, we have used other LIAs that can amplify the amplitude of specific frequency by direct digital synthesizer (DDS), that finds the optimal frequency of surface charge images. In order to confirm the performance of the proposed methods, the electrical properties of lead zirconate titanate (PZT) and triglycine sulfate (TGS) samples were measured. In addition, we compared the performances of the frequency-detection method and the conventional EFM method. Ultimately, enhanced images could be achieved using the frequency-detection method. The optimal modulated frequency-shift for force–gradient measurements was found to be 2 kHz. Additionally, we have shown that it is possible to use a hard cantilever ($K = 42$ N/m, 330 kHz). Therefore, we expect that this technique can be applied to measure the electrical properties of bio-molecular films.

Keywords: electrostatic force microscopy; EFM; direct digital synthesizer; PZT; TGS

1. Introduction

Scanning probe microscopy (SPM) is widely used to analyze the surface structures and properties of semiconductor and bio-molecular films [1–10]. The merits of the SPM method are that it does not require any process for sample preparation, and minimizes damages of the probing sample [11–13]. Moreover, the growth of industries related to semiconductor and nano-bio devices has led to the development of nanotechnology. Many researchers have now become aware of the importance of local surface charge distributions, such as the local doping profiles of semiconductors [11,14,15], the work function of two-dimensional materials [16–18], the surface potentials of bio-molecular films [19–22], and the diodic behavior of nanofluidic devices [23–28]. From this point of view, electrostatic force microscopy (EFM) is convenient when used to monitor the surface charge density levels and energy properties of various films.

The basic principles of EFM are known to be measurements of amplitude changes at a fixed frequency (amplitude modulation, AM) or frequency changes at a fixed amplitude (frequency modulation, FM) of a vibrating cantilever, while maintaining a constant distance between the tip and the surface of the sample. As electrostatic force F_z^{el} is applied via AC voltage (V_{AC}), the probe

vibrates with a frequency of ω . Thus, we can assume that the capacitance C , which is dependent on the probe–sample distance z , is between the probe and the sample. In this case, the electrostatic force F_z^{el} can be written as

$$\begin{aligned} F_z^{el} &= -\frac{1}{2} \frac{\partial C}{\partial z} (V_{DC} - V_{CPD} + V_{AC} \sin \omega t)^2 \\ &= -\frac{1}{2} \frac{\partial C}{\partial z} \left\{ (V_{DC} - V_{CPD})^2 + 2(V_{DC} - V_{CPD})V_{AC} \sin \omega t + V_{AC}^2 \sin^2 \omega t \right\} \end{aligned} \quad (1)$$

where V_{DC} is the bias voltage externally applied to the probe, and V_{CPD} is the contact potential difference (CPD) between the tip and the sample. Given that the electrostatic force is proportional to the square of the voltage, as indicated in the equation above, the vibration contains direct current (DC), ω , and 2ω components. First, the DC component is the static attractive force that exists between the electrodes. Second, the ω component is a force that is applied to the previously described charges via the AC electric field. Third, the 2ω component is a force induced onto the capacitors by sole means of the AC voltage. The ω component disappears when an appropriate bias voltage is applied to the probe in order to cancel out the CPD; i.e., $V_{DC} - V_{CPD} = 0$. The surface potential, or CPD, can be quantitatively measured using the feedback control of V_{DC} to ensure that the ω component is equivalent to zero [2,29–31].

The FM mode refers to the detection method by which the resonance frequency shift of the cantilever is tracked by a self-oscillator or a phase-lock loop (PLL) [2,5,29]. Both topographic and electrostatic signals can be detected by the oscillation of a cantilever near the resonance frequency. Although the modulation voltage of the probe is not in resonance frequency, the electrostatic force can be measured and the electrostatic force induces a shift of the natural resonant frequency ω_0 . These side-bands are extremely sensitive to the electrostatic forces as a result of the large gradient force from the probe apex. The measured signal is proportional to the force gradient, and the relationship can be written as

$$\Delta\omega \approx -\frac{\omega}{2k} \frac{\partial F_z^{el}}{\partial z} = -\frac{\omega}{2k} \frac{\partial^2 C}{\partial z^2} (V_{DC} - V_{CPD})V_{AC} \sin \omega_e t = F_e \sin \omega_e t \quad (2)$$

$$F_e \equiv -\frac{\omega}{2k} \frac{\partial^2 C}{\partial z^2} (V_{DC} - V_{CPD})V_{AC} \quad (3)$$

where $\Delta\omega$ is the modulated resonance frequency, and F_e is the magnitude of the modulated frequency. The frequency-modulated cantilever is deflected by the external force and the motion of the probe can be described as

$$\begin{aligned} x(t) &= A \sin \left(\int_0^t (\omega + F_e \sin(\omega_e t)) dt \right) = A \sin \left(\omega t - \frac{F_e}{\omega_e} \cos(\omega_e t) \right), \quad \left(\text{if } \frac{F_e}{\omega_e} \text{ is small} \right) \\ &\approx A \sin(\omega t) - A \frac{F_e}{\omega_e} \sin(\omega_e t) \cos(\omega t) \\ &= A \sin(\omega t) + \frac{A}{2} \frac{F_e}{\omega_e} \sin((\omega - \omega_e)t) - \frac{A}{2} \frac{F_e}{\omega_e} \sin((\omega + \omega_e)t) \end{aligned} \quad (4)$$

where A is the oscillation amplitude [30–32].

In the former study, Zerweck et al. showed that the side-band frequency sensitive to the force gradient can be generated by modulation frequency, and the lateral resolution of FM mode is higher than its of force-sensitive AM mode [30]. Moreover, Y. Miyahara, et al. reported that the image resolution of Kelvin probe force microscopy could be enhanced by applying AC bias at a specific phase of oscillating force [31]. However, it is not yet well understood the relation between the degree of modulation and the side-band frequency. Thus, in this experiment, we described the convenient method to find the optimized side-band frequency, by tuning external frequency during in situ measurements.

Thus, in this study, we utilize a simple, reliable, and precise EFM method using a direct digital synthesizer (DDS) that modifies the side-band frequency ($f_e = \omega_e/2\pi$) and the oscillation frequency ($f_0 = \omega_0/2\pi$) of the tip. The side-band was formed near the natural frequency of cantilever by coupling

with AC voltage of electrostatic force gradient [29–31]. In the case of conventional EFM method, two LIAs are used in a series to extract the side-band signals. The first lock-in amplifier (LIA) can produce a phase output, and the amplitude of the side-band frequency can be measured by feeding the phase output to the second LIA [32]. However, in current study, the force-gradient signals can be directly detected by feeding the side-band frequency to the external LIA of the EFM as a reference signal. Moreover, the advantage of the side-bands near the natural resonance frequency, lies in the fact that they are independent of the resonant frequency, noise bands, and other interfering resonances. Finally, we are able to produce an accurate side-band frequency using the DDS more easily than when using an analog method.

2. Methods and Results

2.1. Materials and Set-Up

In order to confirm the consistency and reliability of the force gradient method, we used lead zirconate titanate (PZT) and triglycine sulfate (TGS) samples, which are ferroelectric materials with polarization domains [33–37]. Moreover, it is possible to adopt a cantilever with high stiffness and frequency ($K \sim 42$ N/m, 330 kHz) levels, such that it can minimize the effect of humidity and enhance the spatial resolution [19].

As shown in Figure 1, we established an EFM system combined with the DDS, in order to generate more precise side-bands. A custom-built DDS system was inserted in commercial atomic force microscopy (AFM) equipment (nTRACE, Nanofocus Inc., Seoul, Korea). In the DDS circuit, a DDS-based programmable waveform generator (AD9834, Analog Dialogue, Norwood, MA, USA) is used, and it operates at 5.5 V with a 50 MHz clock. SR830 and SR844 LIA (Stanford research systems) are used as the external LIA instead of an internal LIA for EFM. Then, the frequency (f_e) of the AC bias voltage and the frequency (f_o) for mechanical oscillation were regulated by the DDS. Ultimately, a combination of the angular frequencies of ω_o and ω_e results in the side-bands of $\omega_o \pm \omega_e$. As we directly assign a side-band frequency to the EFM lock-in amplifier, the EFM signals can be extracted. Additionally, we were able to optimize the recipe and carry out the various measurements in FM mode, because the side-band frequency of any cantilever is easily generated by the DDS. The great virtues of digital methods are that they generate less noise than analog methods and offer fine frequency resolutions [38].

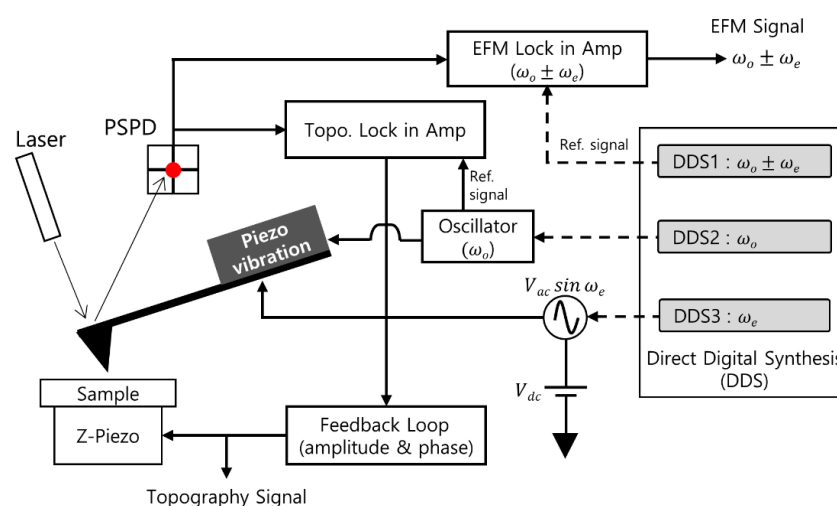


Figure 1. Schematic set-up of the electrostatic force microscopy (EFM) using a direct digital synthesizer (DDS). The vibration of the oscillator with a natural frequency of ω_o , alternating current (AC) voltage with a frequency of ω_e , and EFM signals with a side-band frequency of $\omega_o \pm \omega_e$ were operated by the DDS.

We measured the surface profiles of the zirconate titanate (PZT) and triglycine sulfate (TGS) samples using the conventional EFM method and the modified frequency-detection method. First, the $\text{PbZr}_x\text{Ti}_{1-x}\text{O}_3$ (PZT) films were deposited onto silicon substrates via radio frequency (RF) magnetron sputtering. The polarization direction of each domain in the PZT films was randomly oriented. This enabled us to construct arranged domains on the PZT film by applying positive or negative voltage to the probe [36,39]. Additionally, TGS grown by evaporation from aqueous solution was chosen owing to its natural ferroelectric properties [40].

2.2. Optimal Frequency Detection for EFM Image

Evaluations for image quality were performed using calculation of signal-to-noise ratio (SNR). The root mean square (RMS) noise can be defined as the square root of the mean variances from the pedestal region. Hence, the SNR can be written as follows:

$$\text{SNR} = \text{signal}/\text{RMS noise} \quad (5)$$

Subsequently, we investigated various side-band frequencies for the optimization of the recipe using the DDS method. In this experiment, a commercial Pt/Ir-coated EFM tip with a force constant of 2.8 N/m and resonance frequency of 75 kHz (PPP-EFM, NANOSENSORSTM, Neuchâtel, Switzerland) was used. As shown in Figure 2, we obtained various EFM images of the TGS surface using both of typical and modified methods. All measurements were carried out at the same position to directly compare the image qualities. Each image was drawn using SPIP software (version 6.3.2, Image Metrology, Hørsholm, Denmark) and the SNR was analyzed using Matlab software. The frequency-shift of side-band was varied from 1 to 5 kHz. When we used a spectrum analyzer (HP 8596E, Hewlett-Packard, Palo Alto, CA, USA), it was possible to obtain the maximum SNR at a 2 kHz side-band difference; this value was approximately 2.6 times higher than the result of the lowest SNR value, as shown in Figure 2e.

2.3. Applications of Optimized Side-Band Frequency

As shown in Figure 3, by taking into account the side-band frequency as a reference signal of the FM mode, we set the optimal frequency shift to be 2 kHz and acquired the TGS images using EFM set-up using DDS. Comparison with conventional AM mode was performed in our set-up because it is difficult to find the same probing spot using standard EFM. In this experiment, the resonance frequency of the cantilever was 66.7 kHz and the spring constant was about 3 N/m. Therefore, the generated side-band frequencies for the FM mode were 64.7 kHz and 62.7 kHz, respectively. In this case, the SNR produced by the optimized frequency also showed 1.73 times higher than that seen with the image of 4 kHz frequency shift, and 1.35 times higher than the AM method.

We also implemented the DDS method with a stiff cantilever (PPP-NCHR, NANOSENSORSTM, Neuchâtel, Switzerland, $K \sim 42$ N/m, 330 kHz) using the DDS method because this allows the generation of the optimized side-band frequency (2 kHz shift). Gold film with a thickness of 15 nm was coated onto a silicon probe using an e-gun evaporator (VI-43N, Anelva, Kanagawa, Japan) to impart conductivity to the tip. With the deposition of Au, the resonance frequency of the cantilever changed slightly ($\omega_0 \sim 314$ kHz).

Surface dipole moment of PZT can be altered by direct contact EFM. Thus, the PZT was chosen to make narrow patterns showing electric contrasts. As shown in Figure 4a, we applied positive bias at 10 V to the dark lines and negative bias at -5 V to the gray line in order to accomplish the domain switching of polarization via an external electric field.

When we measured the surface profiles of the PZT film using the AM mode and optimized side-band mode, the SNR values were found to be 6.0295 and 12.104, respectively. For the TGS sample, the SNR values were calculated to be 4.701 and 7.377. That is, the resolution of the optimized side-band EFM images is improved from 1.57 to nearly twofold compared to that of the AM mode

images. Therefore, the frequency-detection method also can be applied to a high-frequency cantilever to improve the image quality.

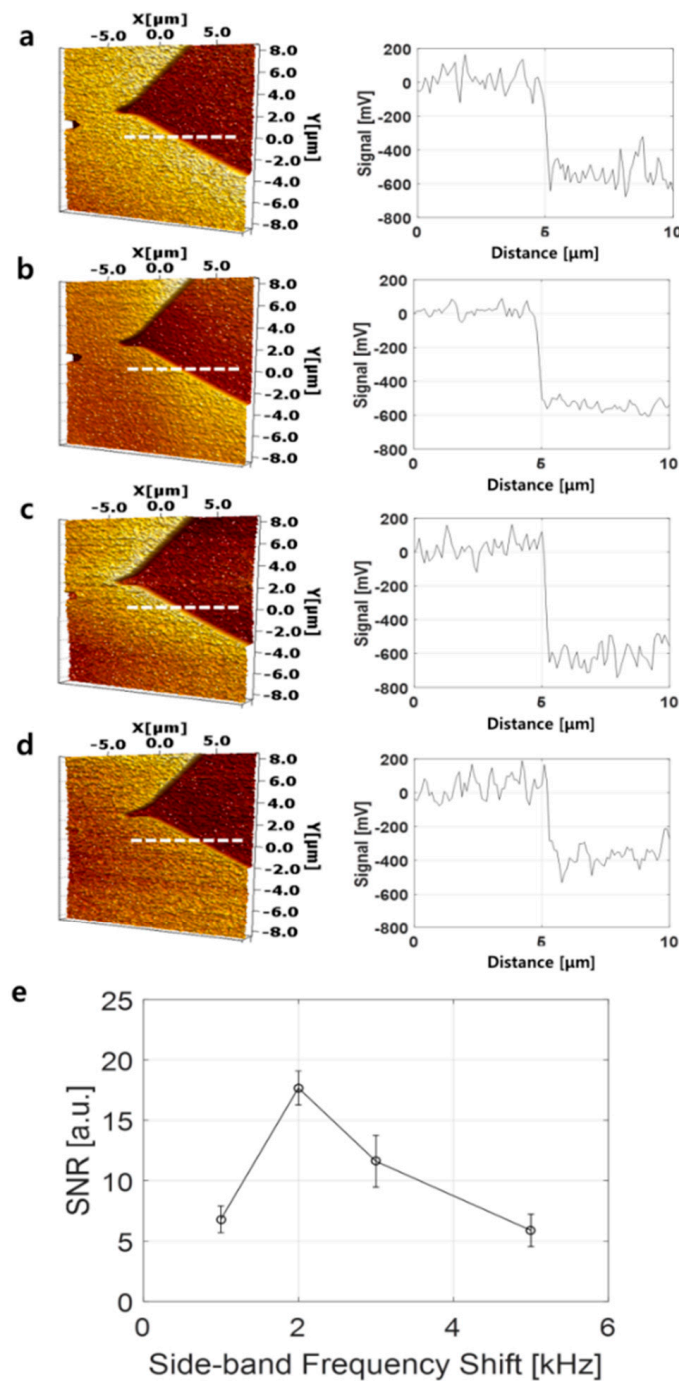


Figure 2. EFM images of the triglycine sulfate (TGS) surface with a scan size of $17 \mu\text{m} \times 17 \mu\text{m}$, showing spontaneous polarization: (a) 1 kHz, (b) 2 kHz, (c) 3 kHz, and (d) 5 kHz side-band frequency shift images using the DDS method and plots of the dashed line. (e) Signal-to-noise ratio (SNR) graph with different side-band frequencies.

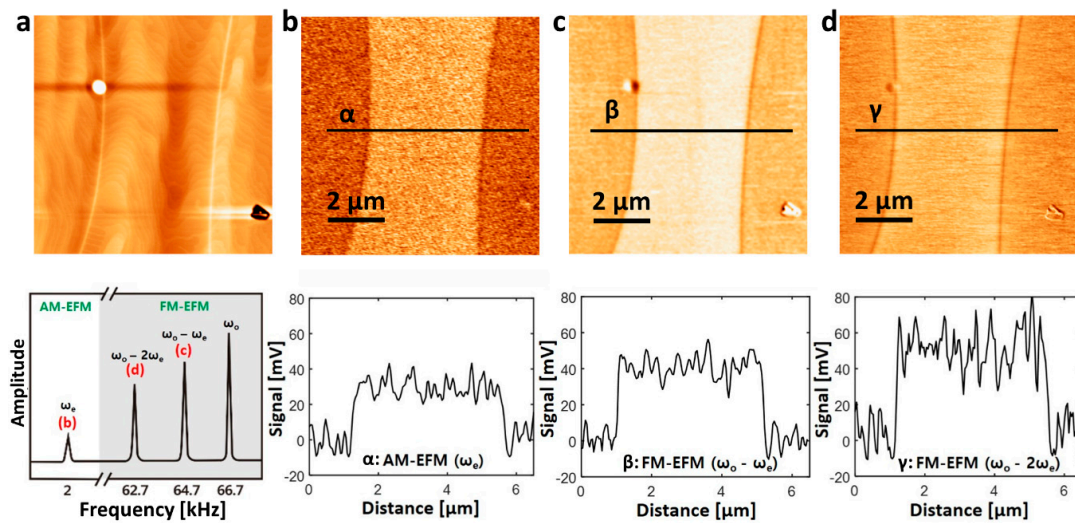


Figure 3. Applied optimal frequency using EFM set-up. Images of triglycine surface (TGS) in $10 \mu\text{m} \times 10 \mu\text{m}$ scan size. (a) The topographic image; (b) AM mode image and line profile (ω_e : 2 kHz, SNR: 6.5735); (c) FM-EFM image and line profile ($\omega_0 - \omega_e$: 64.7 kHz, SNR: 8.8943); (d) FM-EFM image and line profile ($\omega_0 - 2\omega_e$: 62.7 kHz, SNR: 5.1456); FM: frequency modulation; AM: amplitude modulation.

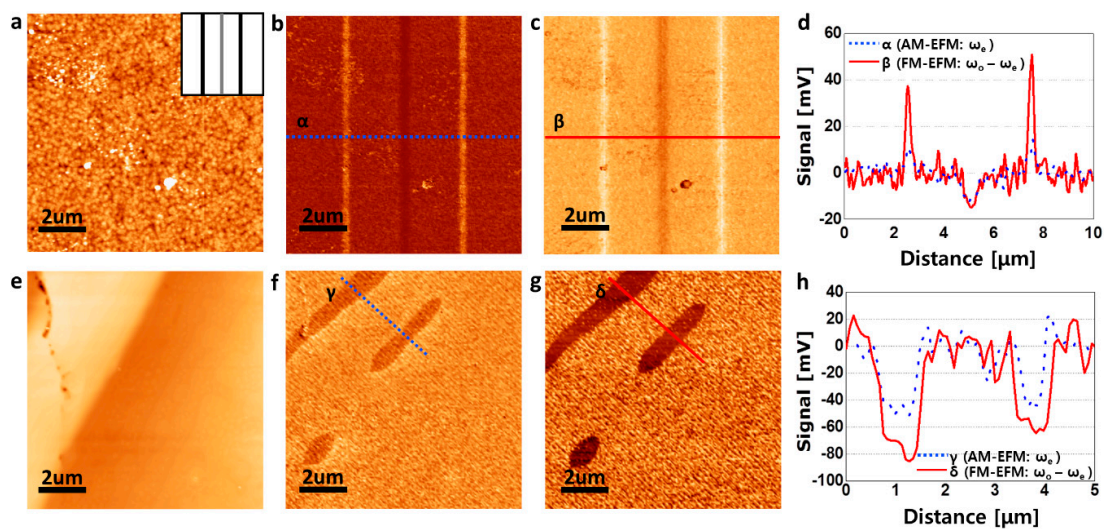


Figure 4. Applied optimal frequency to hard cantilever. EFM images of lead zirconate titanate (PZT) and triglycine surfaces (TGS) in a $10 \mu\text{m} \times 10 \mu\text{m}$ scan size at a high resonance frequency (ω_0 : 314 kHz). (a) Topographic image of PZT (inset: the external field distribution), (b) typical AM-EFM image of PZT (ω_e : 2 kHz), (c) FM-EFM image of PZT at optimized side-band frequency ($\omega_0 - \omega_e$: 312 kHz), (d) line profile of the PZT surface; (e) Topographic image of TGS, (f) typical AM-EFM image of TGS (ω_e : 2 kHz), (g) FM-EFM image of TGS at optimized side-band frequency ($\omega_0 - \omega_e$: 312 kHz) and (h) line profile of the TGS surface.

3. Discussion and Conclusions

In conclusion, we implemented an easy, reliable, and precise frequency detection method using a DDS. Basically, it is known that high quality factor can be achieved by using the side-band close to the resonance frequency. Thus, in this experiment, we found that the appropriate frequency shift having the highest signal-to-noise ratio was 2 kHz by producing precise modulation frequencies. Especially in the TGS measurements conducted here, the SNR is roughly 2.6 times better than the

lowest SNR. Additionally, the results with a stiff cantilever, which is less affected by the humidity on the sample [19], also indicate that the DDS approach is feasible at high frequencies in the FM mode. Ultimately, the EFM images at the optimized side-band frequency are 1.57 to 2 times better than the conventional EFM images. We expect that the findings of our research will help to inspire an accurate and reliable methodology that can be used to analyze the electric characteristics of semiconductor and bio-molecular films.

Acknowledgments: This work was supported by Korea Research Institute of Standards and Science (KRISS) under the project “Development of core measurement technologies for the next generation of nanodevices” (Grant No. 17011063) and Korea Basic Science Institute (KBSI) (Grant No. D37613).

Author Contributions: J.-H. Kim and C.H. Shin conceived and designed the experiments; S. Moon, K.-R. Park, and C.H. Shin performed the experiments; S. Moon, M. Kang, K.-R. Park, and J.-H. Kim analyzed the data; S. Moon wrote the paper. All authors read and approved the final manuscript.

Conflicts of Interest: The authors declare no conflict of interest.

References

1. Jacobs, H.; Knapp, H.; Müller, S.; Stemmer, A. Surface potential mapping: A qualitative material contrast in spm. *Ultramicroscopy* **1997**, *69*, 39–49. [[CrossRef](#)]
2. Melitz, W.; Shen, J.; Kummel, A.C.; Lee, S. Kelvin probe force microscopy and its application. *Surf. Sci. Rep.* **2011**, *66*, 1–27. [[CrossRef](#)]
3. Bottomley, L.A. Scanning probe microscopy. *Anal. Chem.* **1998**, *70*, 425–476. [[CrossRef](#)]
4. Hansma, H.G.; Hoh, J.H. Biomolecular imaging with the atomic force microscope. *Annu. Rev. Biophys. Biomol. Struct.* **1994**, *23*, 115–140. [[CrossRef](#)] [[PubMed](#)]
5. Albrecht, T.; Grütter, P.; Horne, D.; Rugar, D. Frequency modulation detection using high-q cantilevers for enhanced force microscope sensitivity. *J. Appl. Phys.* **1991**, *69*, 668–673. [[CrossRef](#)]
6. Nonnenmacher, M.; O’Boyle, M.; Wickramasinghe, H.K. Kelvin probe force microscopy. *Appl. Phys. Lett.* **1991**, *58*, 2921–2923. [[CrossRef](#)]
7. Gaub, B.M.; Müller, D.J. Mechanical stimulation of piezo1 receptors depends on extracellular matrix proteins and directionality of force. *Nano Lett.* **2017**, *17*, 2064–2072. [[CrossRef](#)] [[PubMed](#)]
8. Yin, F.; Park, S.-H.; Shin, H.-K.; Kwon, Y.-S. Study of hemoglobin-octadecylamine lb film formation and deposition by compressibility analyse, qcm and afm. *Curr. Appl. Phys.* **2006**, *6*, 728–734. [[CrossRef](#)]
9. Kafle, K.; Xi, X.; Lee, C.M.; Tittmann, B.R.; Cosgrove, D.J.; Park, Y.B.; Kim, S.H. Cellulose microfibril orientation in onion (*Allium cepa* L.) epidermis studied by atomic force microscopy (afm) and vibrational sum frequency generation (sfg) spectroscopy. *Cellulose* **2014**, *21*, 1075–1086. [[CrossRef](#)]
10. Hong, J.; Park, S.-i.; Khim, Z. Measurement of hardness, surface potential, and charge distribution with dynamic contact mode electrostatic force microscope. *Rev. Sci. Instrum.* **1999**, *70*, 1735–1739. [[CrossRef](#)]
11. Henning, A.K.; Hochwitz, T.; Slinkman, J.; Never, J.; Hoffmann, S.; Kaszuba, P.; Daghljan, C. Two-dimensional surface dopant profiling in silicon using scanning kelvin probe microscopy. *J. Appl. Phys.* **1995**, *77*, 1888–1896. [[CrossRef](#)]
12. Jiang, J.; Krauss, T.D.; Brus, L.E. Electrostatic force microscopy characterization of trioctylphosphine oxide self-assembled monolayers on graphite. *J. Phys. Chem. B* **2000**, *104*, 11936–11941. [[CrossRef](#)]
13. Shin, C.; Kim, K.; Kim, J.; Ko, W.; Yang, Y.; Lee, S.; Jun, C.S.; Kim, Y.S. Fast, exact, and non-destructive diagnoses of contact failures in nano-scale semiconductor device using conductive afm. *Sci. Rep.* **2013**, *3*, 2088. [[CrossRef](#)] [[PubMed](#)]
14. Tanimoto, M.; Vatel, O. Kelvin probe force microscopy for characterization of semiconductor devices and processes. *J. Vac. Sci. Technol. B Nanotechnol. Microelectron.* **1996**, *14*, 1547–1551. [[CrossRef](#)]
15. Rosenwaks, Y.; Shikler, R.; Glatzel, T.; Sadewasser, S. Kelvin probe force microscopy of semiconductor surface defects. *Phys. Rev. B Cover. Condens. Matter Mater. Phys.* **2004**, *70*, 085320. [[CrossRef](#)]
16. Singh, A.; Guha, P.; Panwar, A.K.; Tyagi, P.K. Estimation of intrinsic work function of multilayer graphene by probing with electrostatic force microscopy. *Appl. Surf. Sci.* **2017**, *402*, 271–276. [[CrossRef](#)]

17. Ziegler, D.; Gava, P.; Güttinger, J.; Molitor, F.; Wirtz, L.; Lazzeri, M.; Saitta, A.; Stemmer, A.; Mauri, F.; Stampfer, C. Variations in the work function of doped single- and few-layer graphene assessed by kelvin probe force microscopy and density functional theory. *Phys. Rev. B Cover. Condens. Matter Mater. Phys.* **2011**, *83*, 235434. [CrossRef]
18. Filleter, T.; Emtsev, K.; Seyller, T.; Bennewitz, R. Local work function measurements of epitaxial graphene. *Appl. Phys. Lett.* **2008**, *93*, 133117. [CrossRef]
19. Moores, B.; Hane, F.; Eng, L.; Leonenko, Z. Kelvin probe force microscopy in application to biomolecular films: Frequency modulation, amplitude modulation, and lift mode. *Ultramicroscopy* **2010**, *110*, 708–711. [CrossRef] [PubMed]
20. Sinensky, A.K.; Belcher, A.M. Label-free and high-resolution protein/DNA nanoarray analysis using kelvin probe force microscopy. *Nat. Nanotechnol.* **2007**, *2*, 653–659. [CrossRef] [PubMed]
21. Clack, N.G.; Salaita, K.; Groves, J.T. Electrostatic readout of DNA microarrays with charged microspheres. *Nat. Biotechnol.* **2008**, *26*, 825–830. [CrossRef] [PubMed]
22. Drolle, E.; Bennett, W.; Hammond, K.; Lyman, E.; Karttunen, M.; Leonenko, Z. Molecular dynamics simulations and kelvin probe force microscopy to study of cholesterol-induced electrostatic nanodomains in complex lipid mixtures. *Soft Matter* **2017**, *13*, 355–362. [CrossRef] [PubMed]
23. Stein, D.; Kruithof, M.; Dekker, C. Surface-charge-governed ion transport in nanofluidic channels. *Phys. Rev. Lett.* **2004**, *93*, 035901. [CrossRef] [PubMed]
24. Vlasiouk, I.; Siwy, Z.S. Nanofluidic diode. *Nano Lett.* **2007**, *7*, 552–556. [CrossRef] [PubMed]
25. Karnik, R.; Duan, C.; Castelino, K.; Daiguji, H.; Majumdar, A. Rectification of ionic current in a nanofluidic diode. *Nano Lett.* **2007**, *7*, 547–551. [CrossRef] [PubMed]
26. Sparreboom, W.; Van Den Berg, A.; Eijkel, J. Principles and applications of nanofluidic transport. *Nat. Nanotechnol.* **2009**, *4*, 713–720. [CrossRef] [PubMed]
27. Cheng, L.-J.; Guo, L.J. Nanofluidic diodes. *Chem. Soc. Rev.* **2010**, *39*, 923–938. [CrossRef] [PubMed]
28. Guan, W.; Fan, R.; Reed, M.A. Field-effect reconfigurable nanofluidic ionic diodes. *Nat. Commun.* **2011**, *2*, 506. [CrossRef] [PubMed]
29. Glatzel, T.; Sadewasser, S.; Lux-Steiner, M.C. Amplitude or frequency modulation-detection in kelvin probe force microscopy. *Appl. Surf. Sci.* **2003**, *210*, 84–89. [CrossRef]
30. Zerweck, U.; Loppacher, C.; Otto, T.; Grafström, S.; Eng, L.M. Accuracy and resolution limits of kelvin probe force microscopy. *Phys. Rev. B Cover. Condens. Matter Mater. Phys.* **2005**, *71*, 125424. [CrossRef]
31. Miyahara, Y.; Topple, J.; Schumacher, Z.; Grutter, P. Kelvin probe force microscopy by dissipative electrostatic force modulation. *Phys. Rev. Appl.* **2015**, *4*, 054011. [CrossRef]
32. Li, C.; Minne, S.; Hu, Y.; Ma, J.; He, J.; Mittel, H.; Kelly, V.; Erina, N.; Guo, S.; Mueller, T. Peakforce Kelvin Probe Force Microscopy. Available online: https://www.bruker.com/fileadmin/user_upload/8-PDF-Docs/SurfaceAnalysis/AFM/ApplicationNotes/AN140-RevA1-PeakForce_KPFM-AppNote.pdf (accessed on 7 July 2017).
33. Park, H.; Jung, J.; Min, D.-K.; Kim, S.; Hong, S.; Shin, H. Scanning resistive probe microscopy: Imaging ferroelectric domains. *Appl. Phys. Lett.* **2004**, *84*, 1734–1736. [CrossRef]
34. Bruno, E.; De Santo, M.; Castriota, M.; Marino, S.; Strangi, G.; Cazzanelli, E.; Scaramuzza, N. Morphological and electrical investigations of lead zirconium titanate thin films obtained by sol-gel synthesis on indium tin oxide electrodes. *J. Appl. Phys.* **2008**, *103*, 064103. [CrossRef]
35. Likodimos, V.; Orlik, X.; Pardi, L.; Labardi, M.; Allegrini, M. Dynamical studies of the ferroelectric domain structure in triglycine sulfate by voltage-modulated scanning force microscopy. *J. Appl. Phys.* **2000**, *87*, 443–451. [CrossRef]
36. Lee, J.-W.; Park, G.-T.; Park, C.-S.; Kim, H.-E. Enhanced ferroelectric properties of pb (zr, ti) o 3 films by inducing permanent compressive stress. *Appl. Phys. Lett.* **2006**, *88*, 072908. [CrossRef]
37. Gainutdinov, R.; Belugina, N.; Tolstikhina, A.; Lysova, O. Multimode atomic force microscopy of triglycine sulfate crystal domain structure. *Ferroelectrics* **2008**, *368*, 42–48. [CrossRef]
38. Murphy, E.; Slattery, C. Direct Digital Synthesis (dds) Controls Waveforms in Test, Measurement, and Communications. Available online: <http://www.analog.com/en/analog-dialogue/articles/dds-controls-waveforms-in-test.html> (accessed on 7 July 2017).

39. Ren, X. Large electric-field-induced strain in ferroelectric crystals by point-defect-mediated reversible domain switching. *Nat. Mater.* **2004**, *3*, 91–94. [[CrossRef](#)] [[PubMed](#)]
40. Hong, J.; Noh, K.; Park, S.-I.; Kwun, S.; Khim, Z. Surface charge density and evolution of domain structure in triglycine sulfate determined by electrostatic-force microscopy. *Phys. Rev. B Cover. Condens. Matter Mater. Phys.* **1998**, *58*, 5078. [[CrossRef](#)]



© 2017 by the authors. Licensee MDPI, Basel, Switzerland. This article is an open access article distributed under the terms and conditions of the Creative Commons Attribution (CC BY) license (<http://creativecommons.org/licenses/by/4.0/>).